Central European Journal of Energetic Materials
ISSN 1733-7178; e-ISSN 2353-1843

Cent. Eur. J. Energ. Mater. 2020, *17*(3): 451-469; DOI 10.22211/cejem/127934
Article is available in PDF-format, in colour, at:
http://www.wydawnictwa.ipo.waw.pl/cejem/Vol-17-Number3-2020/CEJEM_01115.pdf

Research paper

Study of Ammonium Perchlorate-based Molecular Perovskite ($(H_2DABCO)[NH_4(ClO_4)_3]$)/Graphene Energetic Composite with Insensitive Performance

Yang Liu[1], Li-shuang Hu[1,*], Shida Gong[1], Chunyu Guang[1], Lianqiang Li[2], Shuangqi Hu[1], Peng Deng[1,]**

[1] *School of Environment and Safety Engineering, North University of China, China*
[2] *Institute of Occupational Health of Ordnance Industry, China*
E-mails: * hlsly1314@163.com; ** nash_deng@163.com

Abstract: In order to improve the safety properties of molecular perovskite energetic materials, ammonium perchlorate-based molecular perovskite ($(H_2DABCO)[NH_4(ClO_4)_3]$, DAP)/graphene composite was prepared and characterized. Molecular perovskite DAP was prepared via a molecular assembly strategy by the facile one-pot reaction of triethylenediamine (TEDA, DABCO), perchloric acid, and ammonium perchlorate, and the DAP/graphene composite was fabricated by mechanical mixing with 10 wt.% graphene. The results demonstrated that impact sensitivity (>120 cm), friction sensitivity (25%) and electrostatic spark sensitivity (7.04 J) of the DAP/graphene composite was less sensitive than raw DAP (impact, friction and electrostatic spark sensitivity: 112.3 cm, 45%, and 5.39 J, respectively), due to the composite desensitization mechanism of graphene. This work may offer new ideas for the design and fabrication of insensitive molecular perovskite-based energetic composites.

Keywords: ammonium perchlorate, molecular perovskite, graphene, energetic composite, composite desensitization

1 Introduction

As a hot research topic, molecular perovskite energetic materials have attracted much attention due to their unique structure and distinguished properties [1-5]. Combining an inorganic oxidizer, perchlorate, and an organic fuel, triethylenediamine, into a closely-packed, high-symmetry terniary unit at the molecular level, an inorganic-organic ammonium perchlorate-based molecular perovskite has been introduced into the field of energetic materials as a new developing trend for the design and construction of advanced energetic materials for new applications [6-8]. As one of the most important perchlorate-based molecular perovskites, with excellent performance, ammonium perchlorate (AP)-based molecular perovskite ($(H_2DABCO)[NH_4(ClO_4)_3]$, DAP) can be easily obtained by the simple one-pot reaction of AP, perchloric acid and triethylenediamine (molar ratio: 1:2:1). Compared to nitramine or nitroaromatic explosives [9, 10], such as trinitrotoluene (TNT), octahydro-1,3,5,7-tetranitro-1,3,5,7-tetrazocine (HMX), 2,4,6,8,10,12-hexanitrohexaazatetracyclododecane (HNIW), DAP not only possesses low cost, but also shows better detonation performance (theoretical detonation velocity and pressure: 9.588 $km \cdot s^{-1}$ and 49.4 GPa, respectively). This indicated that it has potential as the next generation of high-energy-density energetic materials as a substitute for traditional explosives in many applications.

Poor safety characteristics, however, have seriously hindered their development in military and civil industries [3]. Molecular perovskite energetic materials with high impact and friction sensitivities will have a severe impact on their potential applications. Thus, an emerging challenge is to regulate the safety characteristics of DAP and reduce the sensitivities to meet actual requirements [11].

Graphene, regarded as an important class of insensitive additive material, can be used to reduce the sensitivity of high sensitivity explosives and enhanced their thermal stability, due to its intrinsic electrical and thermal conductivities [12-15]. From the hot-spot theory of high-energy explosives, hot-spots could be easily formed from local stress-strain to thermal decomposition under external stimuli conditions, resulting in eventual ignition. Graphene mixing desensitization technology can enhance the interfacial interactions between explosives and two-dimensional grapheme materials, and promote the efficient removal of hot-spots from external stimuli by the excellent heat conduction properties of grapheme [16, 17], making the external stimuli insufficient for the ignition of the energetic material. Therefore, it is significant and promising to modify the safety performance of highly sensitive explosives by graphene mixing desensitization

technology [18-21]. What is more, it was found that graphene is regarded, interestingly, as a desensitizer in energetic materials and is greatly beneficial for reducing the mechanical sensitivities of molecular perovskite DAP.

In the present work, graphene was introduced to the design and fabrication of the DAP/graphene energetic composite with reduced sensitivity. The DAP/graphene composite was fabricated by mechanical mixing and characterized by scanning electron microscopy, X-ray diffraction, and Fourier transform infrared spectroscopy. The thermal decomposition behaviour and the kinetics of the thermal decomposition reaction were analyzed. In addition, the safety performance of the as-obtained samples was investigated by impact, friction, and electrostatic spark sensitivity tests. The mixing desensitization mechanism was analyzed for the presence of grapheme nanosheets. The results demonstrated that the mechanical (impact and friction) and electrostatic spark sensitivities of DAP/graphene energetic composite exhibited less sensitive properties than raw DAP. This work may offer new ideas for the design and fabrication of graphene-based molecular perovskite energetic composites with insensitive performance.

2 Experimental Section

2.1 Materials

AP and perchloric acid (liquid, 70%) were provided by Shanxi Jiangyang Chem. Eng. Co. Ltd. The triethylenediamine was obtained from Shanghai Aladdin Bio-Chem Technology Co. Ltd. Graphene (5~10 nm, 99.5%) was obtained from Nanjing Xianfeng NANO Materials Technology Co. Ltd. Deionized water was from our own laboratory.

2.2 Preparation of DAP and DAP/graphene Composite

DAP was synthesized by the molecular assembly strategy [3]. AP (0.1175 g, 0.1 mmol) and triethylenediamine (0.112 g, 0.1 mmol) were added successively to water (20 mL). Perchloric acid (0.163 mL, 0.2 mmol) was then added to the mixture. After heating to obtain complete dissolution, the solution was kept at room temperature. After 7 days, the as-prepared DAP was obtained by filtration. The DAP/graphene composite was prepared by mechanical mixing. DAP (1.8 g) and grapheme (0.2 g) were added to an agate mortar. The energetic composite was obtained by artificial mixing for 30 min.

2.3 Characterization

The morphologies of the samples were observed by scanning electron microscopy (SEM, TESCAN Mira3, Brno, Czechia). The X-ray diffraction (XRD) patterns were recorded on a Philips X'Pert Pro X-ray diffractometer (PANalytical, Holland). Fourier transform infrared (FT-IR) spectra from 4000 to 650 cm^{-1} were collected on a Nicolet 5700 Fourier spectrometer (Thermo Scientific, America) using KBr pellets. Raman spectra were collected on a Raman spectrophotometer (Renishaw, England).

Thermal decomposition performance analysis was carried out on a STA449F3 thermogravimetric-differential scanning calorimeter (TG-DSC, Netzsch, Germany) at a heating rate of 10 $°C \cdot min^{-1}$ with an inert N_2 atmosphere. Based on GJB-772A-1997, the impact sensitivity was tested by a WL-1 type apparatus. The special height (H_{50}) value represents the height from which a 2.0 kg drop-hammer will result in an explosive event in 50% of the trials (sample mass: 30 mg, test number: 20 drops). The friction sensitivity experiments were measured with an MGY-1 type friction sensitivity instrument. A probability of explosion (%) was obtained:

– sample mass: 30 mg,
– sample test: 20 drops,
– pendulum hammer: 2 kg,
– tilt angle: 90°, and
– pressure 3.50 MPa.

The electrostatic spark sensitivities were tested with a JGY-50 type electrostatic sensitivity apparatus.

3 Results and Discussion

Molecular perovskite energetic materials, DAP, were fabricated first by the facile, green one-pot reaction of AP, perchloric acid, and DABCO with a mole ratio of 1:2:1. SEM images of the samples were collected and are shown in Figures 1(a) and 1(b). The molecular structure of DAP is shown in Figure 1(c). Cube-shaped particles of micron-size can be obtained as in Figure 1(b). The side length of a typical sample is about 200 μm, as shown in Figure 1(a). Incomplete morphologies with macroscopic defects were observed clearly in Figure 1(b), because of the unstable room-temperature crystallization environment.

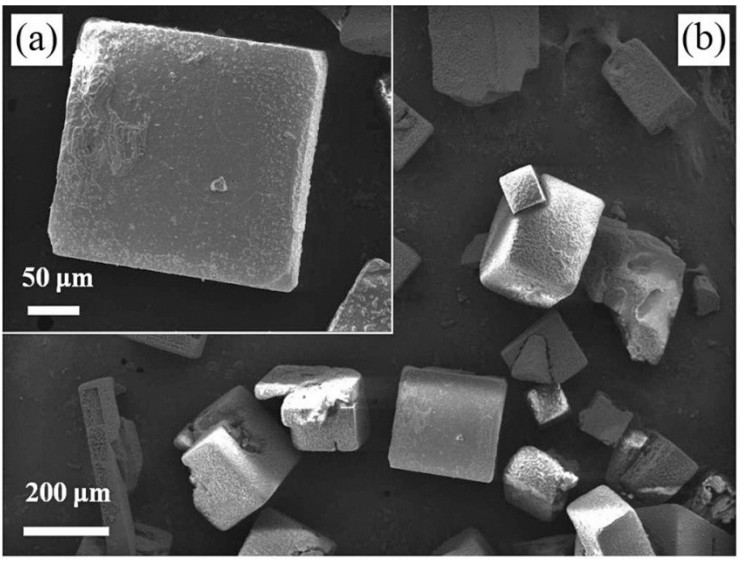

(a, b)

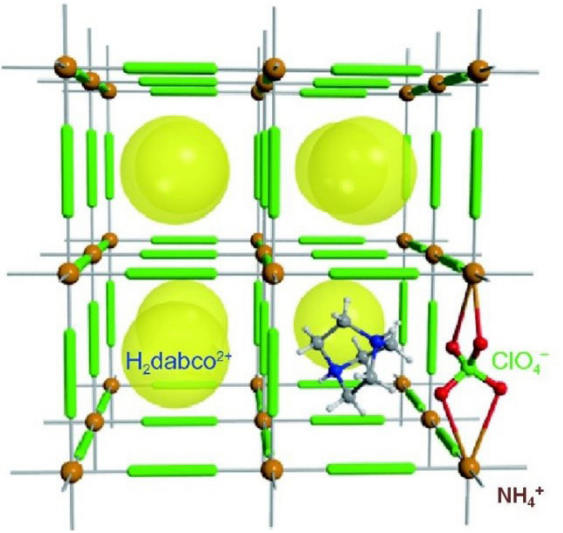

(c)

Figure 1. SEM images of DAP (a, b) and a schematic of its molecular structure (c)

The crystal structure of the as-obtained sample was measured by XRD (Figure 2). Compared with the simulated XRD pattern of (H_2DABCO)[$NH_4(ClO_4)_3$] compound (CCDC: 1528108), the measured XRD pattern is in general agreement with the simulated one. The main diffraction peaks were at 21.44°, 24.67°, 27.7°, 36.88°, and 39.40° reflected from (222), (400), (420), (531), and (600) of the DAP sample, respectively. According to the reported literature [3], the crystal structure of DAP belongs to molecular perovskite stacking structures ABX_3. Protonated H_2DABCO^{2+} is regarded as the A cation in the DAP unit cell, NH_4^+ as the B cation, and ClO_4^- as the X bridges. Each NH_4^+ cation is surrounded by twelve O atoms from six ClO_4^- anions by hydrogen bonding interactions. The ClO_4^- anions can be considered as bridges with two ambient NH_4^+ cations, forming a three-dimensional cage-like supramolecular framework. The protonated H_2DABCO^{2+} is locked in the cubic cage-like space. The above results demonstrated that molecular perovskite DAP had been successfully synthesized by the facile one-pot reaction.

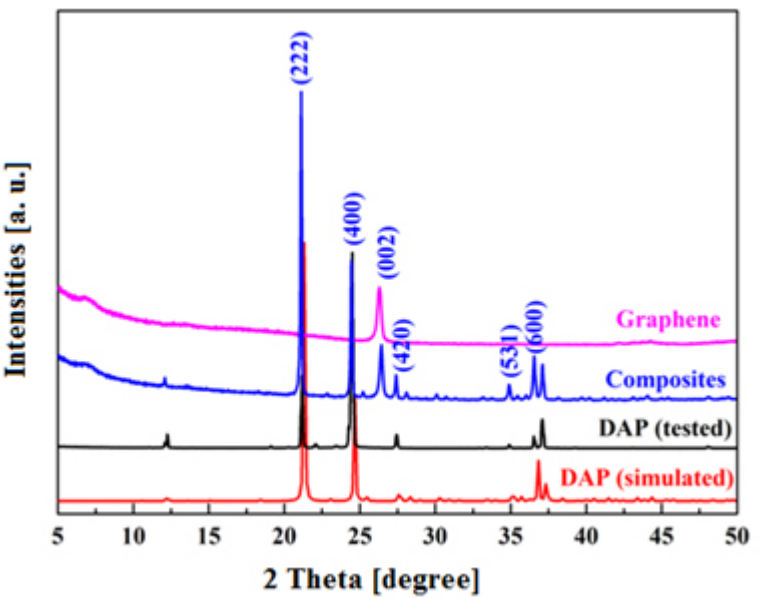

Figure 2. XRD patterns of the samples

The FT-IR spectra are shown in Figure 3(a). The assignment of the FT-IR peaks of the components AP and DABCO, in the as-prepared sample of DAP is as follows. For the AP, the spectrum peaks were located at 619 and 1038 cm^{-1}, corresponded to ClO_4^-, and the peaks at 1410 and 3273 cm^{-1} are from

the NH_4^+ vibration. For the DABCO unit, the main peaks are at 835, 908, and 1056 cm^{-1}, originating from the DABCO skeletal motion. The FT-IR peaks at 3235, 2937, 2870, and 991 cm^{-1} correspond to CH_2, the peaks at 1678 and 1455 cm^{-1} to CH_2, and the peak at 1314 cm^{-1} to C–N. For the FT-IR spectrum of the as-prepared samples, the main oxidant group ClO_4^- was located at 1064 and 627 cm^{-1}, with the DABCO skeletal motion located at 1048, 890, and 850 cm^{-1}; this indicated that the main functional groups existed in the perovskite structure.

The Raman spectrum of DAP samples is shown in Figure 3(b). The Raman characteristic peak at 3192 cm^{-1} is scattered from NH_4^+, and the peaks at 935, 627, and 437 cm^{-1} are from ClO_4^-. The peaks located at 1469, 1284, and 798 cm^{-1} from the protonated H_2DABCO^{2+} correspond with the E_{1g} band of N–C deformation, the E_{1g} band of CH_2 twist/C–N rock, and the A_g band of the CH_2 rock, respectively. The Raman peaks around 2900 cm^{-1} correspond to the C–H stretching vibration. Based on the above spectral analysis, the characterization results also corroborated the successful preparation of molecular perovskite energetic material DAP by the molecular assembly strategy.

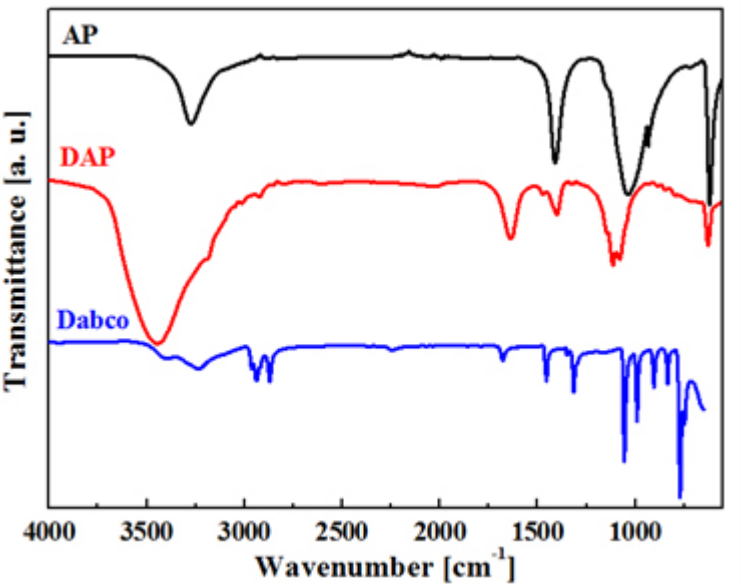

(a)

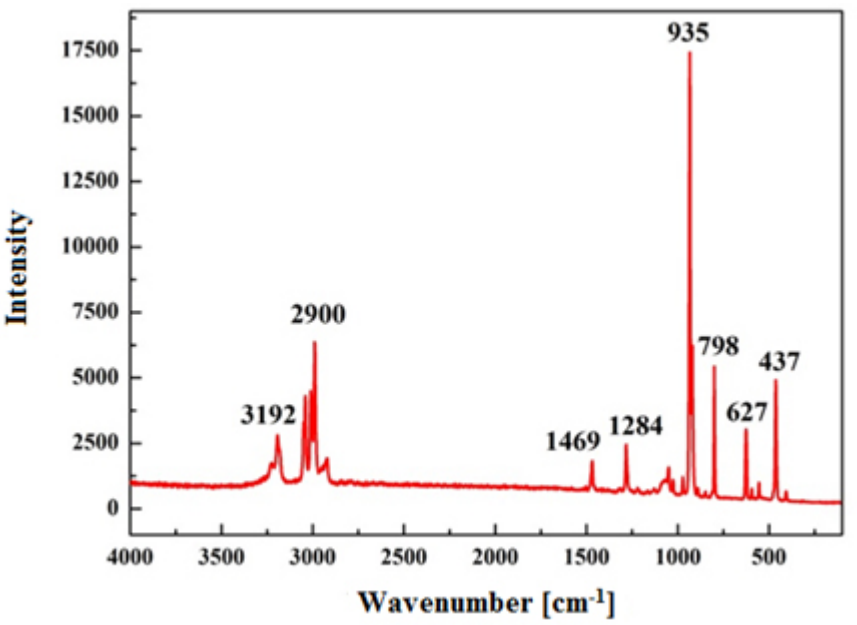

(b)

Figure 3. FT-IR spectra of the samples (a) and Raman spectrum of DAP (b)

The Raman spectrum of graphene in Figure 4 shows the two key characteristic peaks of graphene material, which are located at around 1348 cm^{-1} (the breathing mode of K-point phonons of A_{1g} symmetry, D band) and 1594 cm^{-1} (the in-plane stretching motion of symmetric sp^2 C–C bonds, G band). The I_D:I_G ratio of the graphene materials was numerically equal to 1.17, which is consistent with the literature [22, 23]. A high I_D:I_G ratio revealed that a certain degree of disorder exists in the graphene materials. Graphene nanosheet samples, with a thickness of 10~20 nm, were obtained commercially, as shown in Figure 5. The FT-IR analysis in Figure 6 illustrated a low-quality spectrum because of the strong infrared absorption of graphene. However the main peaks, located at 1700-1580, 1200-1100, and 1000-800 cm^{-1}, corresponded to the stretching vibration of C=C, the stretching vibration of C–C, and the bending vibration of C=C, respectively. The XRD pattern of graphene in Figure 2 also suggested that the main diffraction peak located at 26.2° was reflected from crystal face (002) of graphene.

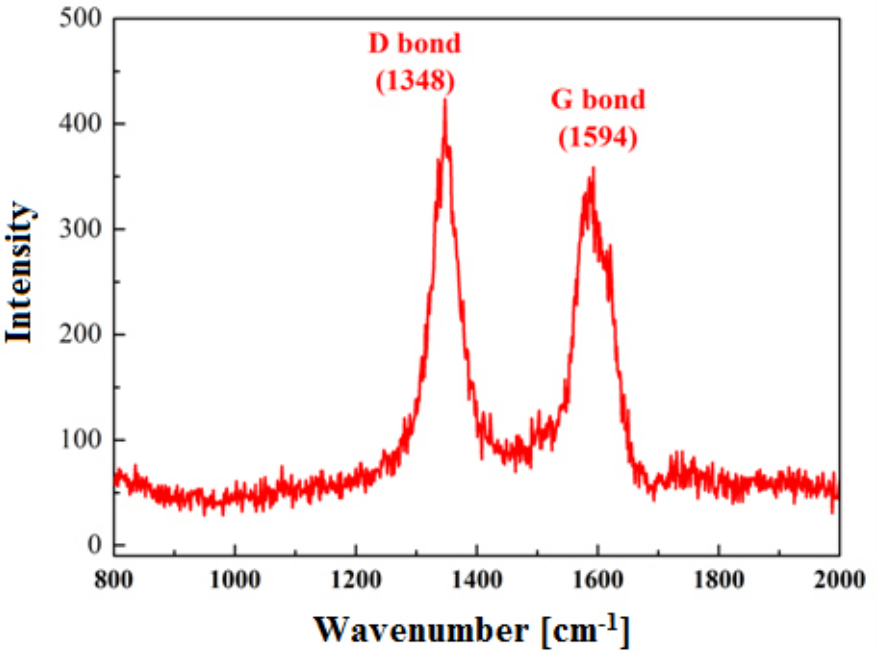

Figure 4. Raman spectrum of graphene nanosheets

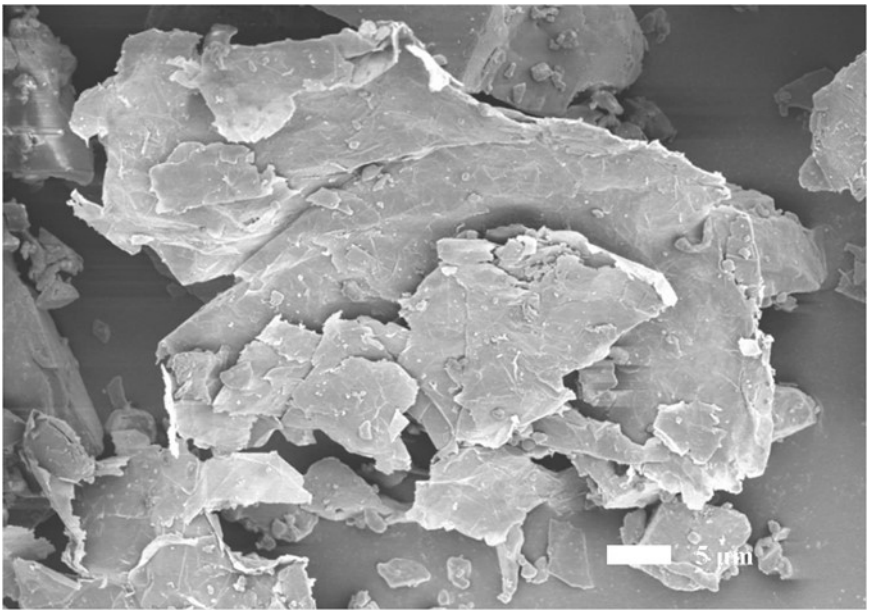

Figure 5. SEM images of graphene

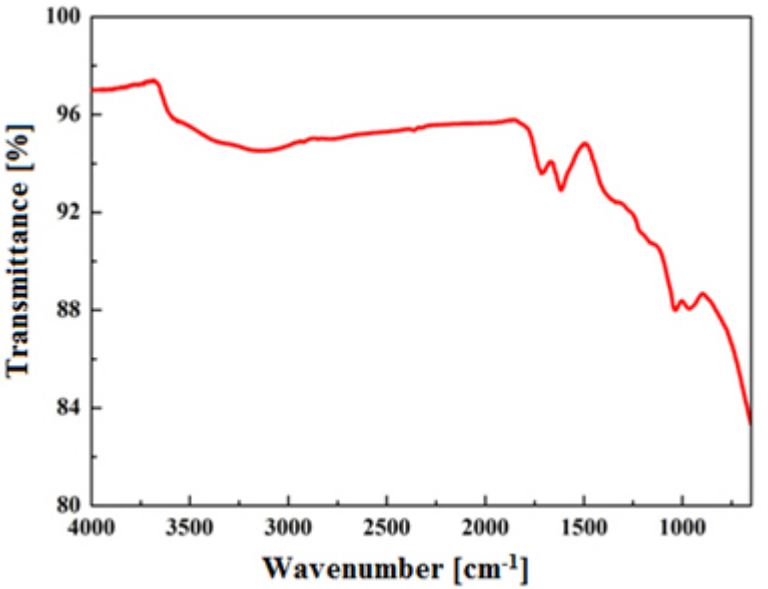

Figure 6. FT-IR spectrum of graphene nanosheets

DAP/graphene composite was prepared by mechanical mixing of DAP with 10 wt.% graphene and then characterized. Figure 7(a) shows the morphology of the composites. Graphene nanosheets with a thickness of 100 nm can be observed, and the DAP particles and graphene nanosheets can be found, marked by green and yellow arrows, respectively. Through mechanical mixing, the sizes of the DAP particles have been reduced, and the graphene nanosheets have been evenly dispersed around the DAP particles, resulting in a good uniform composite system. The FT-IR spectra in Figure 7(b) demonstrate that the composites had been prepared by facile mechanical physical mixing without chemical interactions. The XRD patterns in Figure 2 suggest that the diffraction peaks at 21.04°, 24.38°, 27.30°, 36.45°, and 39.57° are reflected from crystal faces (222), (400), (420), (531), and (600) of the component DAP, respectively. The other diffraction peak at 26.2° revealed the presence of graphene nanosheets in the composite system. The above results showed that the DAP/graphene composite had been successfully prepared by facile physical mixing.

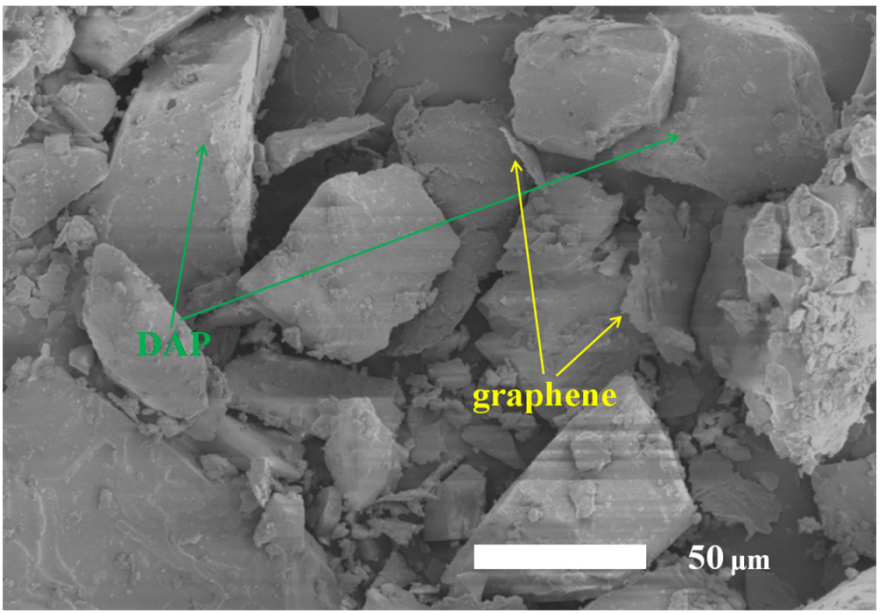

(a)

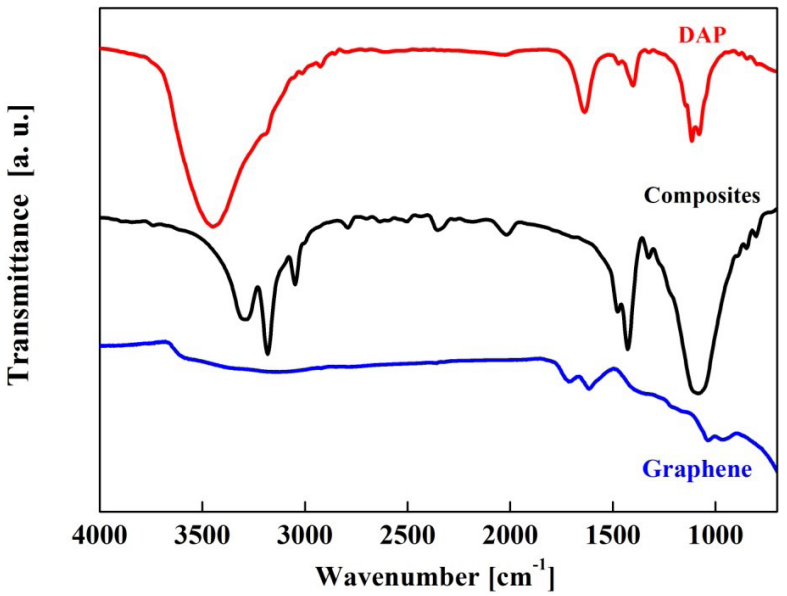

(b)

Figure 7. SEM image of the DAP/graphene composite (a) and FT-IR spectra (b)

The thermal decomposition performance of the samples was investigated by TG-DSC, as shown in Figure 8. Two main peaks, located at 274.5 and 394.4 °C from raw DAP material are considered as the endothermic and the exothermic processes, respectively. The heat released from the thermal decomposition stage could be as high as 4199 $J \cdot g^{-1}$. With graphene nanosheets added, the peak temperature of thermal decomposition of the composite was markedly reduced by 22.1 °C, although the endothermic peak (274.5 °C) remained unchanged. The heat released from the energetic composite was decreased slightly, less than the pure DAP material. In this decomposition process, grapheme nanosheets can react with the oxidizer DAP. However the non-energetic additives in this composite system reduce the total energy release.

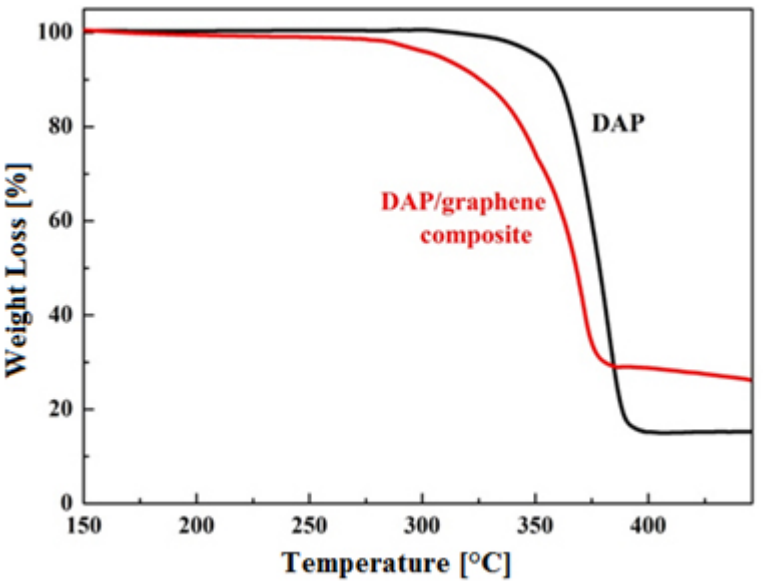

(a)

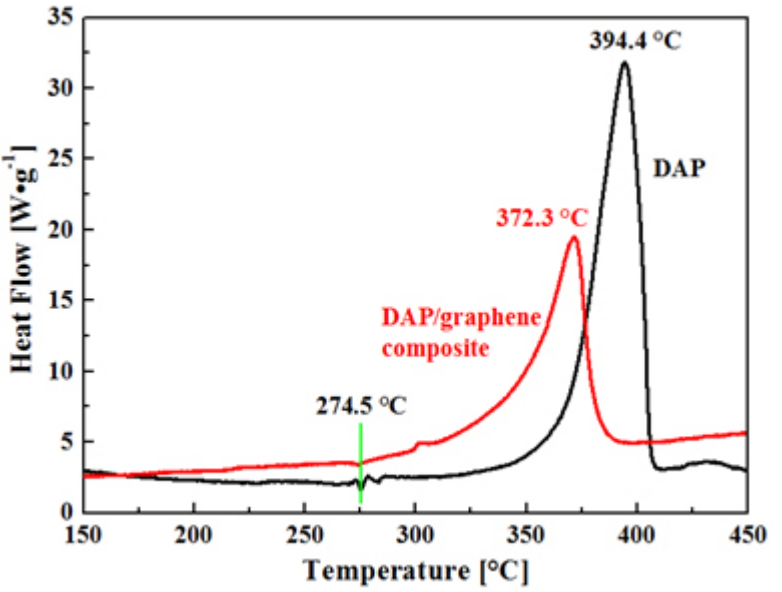

(b)

Figure 8. TG (a) and DSC (b) curves of DAP and the DAP/graphene composite

In order to study the thermal decomposition performance of DAP with graphene nanosheets as additives, the DAP and the DAP/graphene composite were investigated by DSC at different heating rates (Figures 9(a) and 9(b)). From the exothermic peak temperatures as a function of heating rate (Table 1), several important kinetic parameters for the thermal decomposition of DAP and DAP/graphene were calculated by the Kissinger equation (Equation 1) [24]:

$$\ln\left(\frac{\beta}{T_p^2}\right) = \ln\frac{AR}{E_a} - \frac{E_a}{RT_p} \tag{1}$$

where is the heating rate in $K \cdot min^{-1}$, T_p is the peak temperature, A is the frequency factor in s^{-1}, R is the ideal gas constant (8.314 $J \cdot (mol \cdot K)^{-1}$), and E_a is the activation energy.

Table 1. Exothermic peak temperatures (T_p) and activation energy (E_a) of pure DAP and the DAP/graphene composite

Sample	T_p [°C], at heating rate [°C·min^{-1}]				E_a [kJ·mol^{-1}]
	5	10	15	20	
DAP	387.5	394.4	403.9	410.6	205.4
DAP/graphene	348.9	372.3	376.2	381.9	124.1

The experimentally measured ln(/T_p^2) versus 1/T_p for DAP and the DAP/graphene composite is shown in Figure 9(c). For pure DAP material, the activation energy (E_a) of thermal decomposition was calculated to be 205.4 kJ·mol^{-1}, which is higher than HNIW (165.5 kJ·mol^{-1}) and AP (181 kJ·mol^{-1}) [5, 25]. With 10 wt.% nanosheets as additive, the E_a of thermal decomposition of the DAP/graphene composite became 124.1 kJ·mol^{-1}. The occurence of a clear change originated from the additive component, graphene, which can promote H transfer and activate thermal decomposition of DAP [26].

Furthermore, the safety performance (impact, friction and electrostatic spark sensitivity) of the as-prepared samples was investigated and the test results are listed in Table 2. Compared with the value of the special height (H_{50}: 112.3 cm) of the impact sensitivity of raw DAP, the DAP/graphene composite (H_{50} >120 cm) exhibited less sensitivity. For friction sensitivity, the DAP/graphene composite also exhibited less sensitive properties (explosion probability: 25%) than pure DAP (45%). Furthermore, less sensitivity to electrostatic spark was achieved by adding graphene nanosheets. Considering this excellent safety performance, the composite desensitization mechanism of graphene is now discussed.

Table 2. Impact, friction and electrostatic spark sensitivity of DAP and the DAP/graphene energetic composite

Sensitivity	DAP/graphene composite	Raw DAP
Impact sensitivity H_{50} [cm]	>120	112.3
Friction sensitivity [%]	25	45
Electrostatic spark sensitivity [J]	7.04	5.39

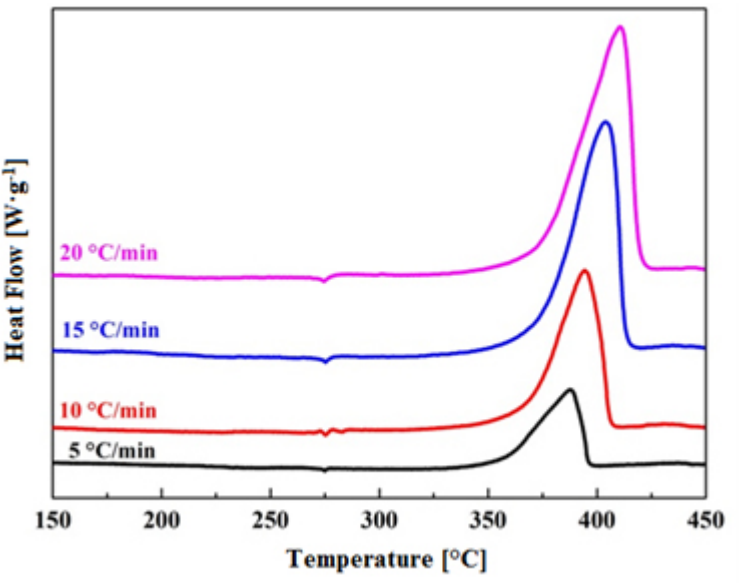

(a)

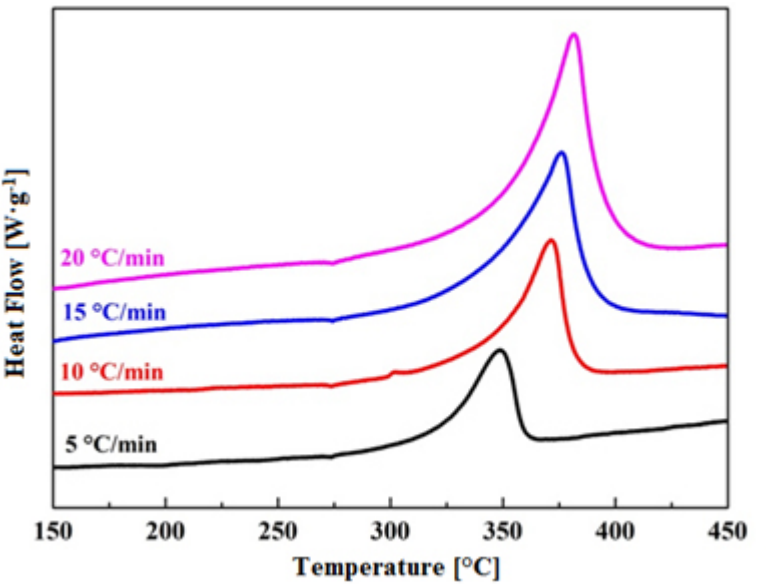

(b)

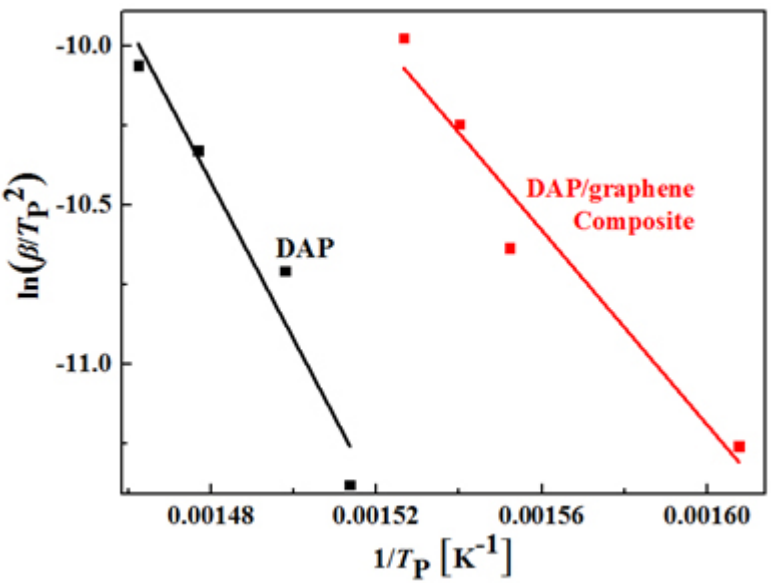

(c)

Figure 9. DSC curves of DAP (a) and the DAP/graphene (b) composite at different heat rates, (c) scatter points are experimental data and lines denote the linear fitting results for the dependence of ln($/T_p^2$) on $1/T_p$ for DAP and the DAP/graphene composite

For mechanical initiation of energetic materials, hot spots could be formed under external mechanical stimuli. For DAP, the mechanical energy acting on the local surfaces of the DAP particles will be transformed into thermal energy, the accumulated thermal energy will trigger the DAP once local overheating exceeds the thermal decomposition threshold of DAP. With graphene added, the thermal conductivity of this system is effectively improved by the two dimensional graphene nanosheets with good heat conduction properties, which will increase the possibility of local heat diffusion. Namely, hot spots can be shifted dependent on the heat conduction path of the graphene nanosheets. In addition, the strong electrical conductivity of graphene nanosheets will improve the overall electron transfer efficiency of the energetic composite and reduce the probability of electrostatic initiation. The above results revealed that the DAP/graphene composite exhibits better applications potential.

4 Conclusions

In summary, graphene was introduced to the design and fabrication of a DAP-based composite. The DAP/graphene energetic composite was prepared by adding 10 wt.% graphene, and was then characterized. The mechanical sensitivity (impact and friction sensitivity: >120 cm and 25%, respectively) and electrostatic spark sensitivity (7.04 J) of the DAP/graphene composite showed greater insensitivity than DAP (impact, friction and electrostatic spark sensitivity: 112.3 cm, 45%, and 5.39 J, respectively), resulting from the mixing desensitization mechanism of graphene. The DAP/graphene energetic composite maybe have better applications potential in the field of energetic materials.

Acknowledgments

The authors thank Prof. Weixiong Zhang and Dr. Shaoli Chen (School of Chemistry, Sun Yat-Sen University) for their support and help.

References

[1] Chen, S.; Shang, Y.; He, C.; Sun, L.; Ye, Z.; Zhang, W.; Chen, X. Optimizing the Oxygen Balance by Changing the A-site Cations in Molecular Perovskite High-energetic Materials. *CrystEngComm* **2018**, *20*(46): 7458-7463.

[2] Zhou, J.; Ding, L.; Zhao, F.; Wang, B.; Zhang, J. Thermal Studies of Novel Molecular Perovskite Energetic Material $(C_6H_{14}N_2)[NH_4(ClO_4)_3]$. *Chinese Chem. Lett*. **2020**, *31*(2), 554-558.

[3] Chen, S.; Yang, Z.; Wang, B.; Shang, Y.; Sun, L.; He, C.; Zhou, H.; Zhang, W.; Chen, X. Molecular Perovskite High-energetic Materials. *Sci. China Mater*. **2018**, *61*(8): 1123-1128.

[4] Shang, Y.; Huang, R.; Chen, S.; He, C.; Yu, Z.; Ye, Z.; Zhang, W.; Chen, X. Metal-free Molecular Perovskite High-energetic Materials. *Cryst. Growth Des.* **2020**, *20*(3): 1891-1897.

[5] Deng, P.; Wang, H.; Yang, X.; Ren, H.; Jiao, Q. Thermal Decomposition and Combustion Performance of High-energy Ammonium Perchlorate-based Molecular Perovskite. *J. Alloy Compd.* **2020**, *827*: 154257.

[6] Jia, Q.; Bai, X.; Zhu, S.; Cao, X.; Deng, P.; Hu, L. Fabrication and Characterization of Nano $(H_2dabco)[K(ClO_4)_3]$ Molecular Perovskite by Ball Milling. *J. Energ. Mater*. **2019**: 1-9.

[7] Li, X.; Hu, S.; Cao, X.; Hu, L.; Deng, P.; Xie, Z. Ammonium Perchlorate-based Molecular Perovskite Energetic Materials: Preparation, Characterization, and Thermal Catalysis Performance with MoS_2. *J. Energ. Mater.* **2020**, *38*(2): 162-169.

[8] Jia, Q.; Deng, P.; Li, X.; Hu, L.; Cao, X. Insight into the Thermal Decomposition Properties of Potassium Perchlorate ($KClO_4$)-based Molecular Perovskite. *Vacuum* **2020**, *175*: 109257.
[9] Bolton, O.; Matzger, A. Improved Stability and Smart-material Functionality Realized in an Energetic Cocrystal. *Angew. Chem., Int. Ed*. **2011**, *123*(38): 9122-9125.
[10] Li, S.; Wang, Y.; Qi, C.; Zhao, X.; Zhang, J.; Zhang, S.; Pang, S. 3D Energetic Metal-organic Frameworks: Synthesis and Properties of High Energy Materials. *Angew. Chem., Int. Ed*. **2013**, *52*(52): 14031-14035.
[11] Deng, P.; Jiao, Q.; Ren, H. Synthesis of Nitrogen-doped Porous Hollow Carbon Nanospheres with a High Nitrogen Content: A Sustainable Synthetic Strategy Using Energetic Precursors. *Sci. Total Environ.* **2020**, *714*: 136725.
[12] Lei, J.; Liu, H.; Yin, D.; Zhou, L.; Liu, J.; Chen, Q.; Cui, X.; He, R.; Duan, T.; Zhu, W. Boosting the Loading of Metal Single Atoms via a Bioconcentration Strategy. *Small* **2020**, *16*(10): 1905920.
[13] Deng, P.; Liu, Y.; Luo, P.; Wang, J.; Liu, Yu.; Wang, D.; He, Y. Two-steps Synthesis of Sandwich-like Graphene Oxide/LLM-105 Nanoenergetic Composites Using Functionalized Grapheme. *Mater. Lett.* **2017**, *194*: 156-159.
[14] Thiruvengadathan, R.; Chung, S.; Basuray, S.; Balasubramanian, B.; Staley, C.; Gangopadhyay, K.; Gangopadhyay, S. A Versatile Self-assembly Approach toward High Performance Nanoenergetic Composite Using Functionalized Graphene. *Langmuir* **2014**, *30*(22): 6556-6564.
[15] Lei, J.; Guo, Q.; Yin, D.; Cui, X.; He, R.; Duan, T.; Zhu, W. Bioconcentration and Bioassembly of N/S Co-doped Carbon with Excellent Stability for Supercapacitors. *Appl. Surf. Sci.* **2019**, *488*: 316-325.
[16] Yan, Q.; Gozin, M.; Zhao, F.; Cohen, A.; Pang. S. Highly Energetic Compositions Based on Functionalized Carbon Nanomaterials. *Nanoscale* **2016**, *8*(9): 4799-4851.
[17] Yu, L.; Ren, H.; Guo, X.; Jiang, X.; Jiao, J. A Novel ε-HNIW-based Insensitive High Explosive Incorporated with Reduced Graphene Oxide. *J. Therm. Anal. Calorim*. **2014**, *117*(3): 1187-1199.
[18] Fleming, K. Hazard Assessments of Energetic Systems, a Field Still in Development. *Propellants, Explos., Pyrotech*. **2018**, *43*(5): 433-435.
[19] Deng, P.; Xu, J.; Li, S.; Huang, S.; Zhang, H.; Wang, J.; Liu, Y. A Facile One-pot Synthesis of Monodisperse Hollow Hexanitrostilbenepiperazine Compound Microspheres. *Mater. Lett*. **2018**, *214*: 45-49.
[20] Li, R.; Wang, J.; Shen, J.; Hua, C.; Yang, G. Preparation and Characterization of Insensitive HMX/Graphene Oxide Composites. *Propellants, Explos., Pyrotech*. **2013**, *38*(6): 798-804.
[21] Liu, T.; Geng, C.; Zheng, B.; Li, S.; Luo, G. Encapsulation of Cyclotetramethylenetetranitramine (HMX) by Electrostatically Self-assembled Graphene Oxide for Desensitization. *Propellants, Explos., Pyrotech*. **2017**, *42*(9): 1057-1065.
[22] Zhang, J.; Wang, X.; Qi, G.; Li, B.; Song, Z.; Jiang, H.; Zhang, X.; Qiao, J. A Novel

N-Doped Porous Carbon Microsphere Composed of Hollow Carbon Nanospheres. *Carbon* **2016**, *96*: 864-870.

[23] Wang, Y.; Zou, H.; Zeng, S.; Pan, Y.; Wang, R.; Wang, X.; Sun, Q.; Zhang, Z.; Qiu, S. A One-step Carbonization Route Towards Nitrogen-doped Porous Carbon Hollow Spheres with Ultrahigh Nitrogen Content for CO_2 Adsorption. *Chem. Commun.* **2015**, *51*(62): 12423-12436.

[24] Hu, L.; Liu, Y.; Hu, S.; Wang, Y. 1T/2H Multi-phase MoS_2 Heterostructure: Synthesis, Characterization and Thermal Catalysis Decomposition of Dihydroxylammonium 5,5′-Bistetrazole-1,1′-diolate. *New J. Chem*. **2019**, *43*(26): 10434-10441.

[25] Chen, J.; He, S.; Huang, B.; Wu, P.; Qiao, Z.; Wang, J.; Zhang, L.; Yang, G.; Huang, H. Enhanced Thermal Decomposition Properties of CL-20 through Space-confining in Three-dimensional Hierarchically Ordered Porous Carbon. *ACS Appl. Mater. Interfaces* **2017**, *9*(12): 10684-10691.

[26] Han, K.; Zhang, X.; Deng, P.; Jiao, Q.; Chu, E. Study of the Thermal Catalysis Decomposition of Ammonium Perchlorate-based Molecular Perovskite with Titanium Carbide MXene. *Vacuum* **2020**, *180*: 109572.

Received: January 8, 2019
Revised: September 26, 2020
First published online: September 28, 2020